Supertransport by Superclimbing Dislocations in ^{4}He: When All Dimensions Matter

Anatoly B. Kuklov[,1] Lode Pollet[,2,3,4] Nikolay V. Prokof'ev[,5] and Boris V. Svistunov[5,4]

[1]*Department of Physics and Astronomy, College of Staten Island and the Graduate Center of CUNY, Staten Island, New York 10314, USA*

[2]*Arnold Sommerfeld Center for Theoretical Physics, University of Munich, Theresienstrasse 37, 80333 München, Germany*

[3]*Munich Center for Quantum Science and Technology (MCQST), Schellingstrasse 4, 80799 München, Germany*

[4]*Wilczek Quantum Center, School of Physics and Astronomy and T.D. Lee Institute, Shanghai Jiao Tong University, Shanghai 200240, China*

[5]*Department of Physics, University of Massachusetts, Amherst, Massachusetts 01003, USA*

The unique superflow-through-solid effect observed in solid ^{4}He and attributed to the quasi-one-dimensional superfluidity along the dislocation cores exhibits two extraordinary features: (i) an exponentially strong suppression of the flow by a moderate increase in pressure and (ii) an unusual temperature dependence of the flow rate with no analogy to any known system and in contradiction with the standard Luttinger liquid paradigm. Based on *ab initio* and model simulations, we argue that the two features are closely related: Thermal fluctuations of the shape of a superclimbing edge dislocation induce large, correlated, and asymmetric stress fields acting on the superfluid core. The critical flux is most sensitive to strong rare fluctuations and hereby acquires a sharp temperature dependence observed in experiments.

Introduction.—A pure (free of ^{3}He impurities) but structurally imperfect crystal of ^{4}He is a highly nontrivial system demonstrating a variety of unique phenomena taking place at temperatures $T \lesssim 0.5$ K that likely persist down to absolute zero: (i) the superflow through solid (STS) [1–8], (ii) the anomalous isochoric compressibility (also known as the syringe effect), which is the thresholdless matter accumulation inside the solid in response to small chemical potential changes that always accompanies the STS [1], and (iii) the giant plasticity [9]. All three features are attributed to highly unusual and essentially quantum properties of dislocations.

The STS effect is explained by superfluidity in the cores of certain dislocations, as established for both the screw and edge dislocations by *ab initio* path integral simulations in Refs. [10,11]; the original idea that dislocations in ^{4}He might have superfluid cores goes back to the work by Shevchenko [12]. The only existing scenario explaining the syringe effect is based on superclimb of edge dislocations [11]. In contrast to the conventional climb assisted by pipe diffusion of thermally activated vacancies along the dislocation core [13,14] (viable only at high temperature), the superclimb is assisted by the superflow along the core. The syringe effect persisting down to low temperatures when thermal activation is no longer possible, as well as first-principle simulations of edge dislocations demonstrating superclimb, provide strong support to the minimalistic unified scenario behind all phenomena based on the (quantum-)rough edge dislocations with superfluid cores.

Since dislocation cores are quasi-one-dimensional objects, it is natural to expect that their superfluid properties fit the Luttinger liquid (LL) paradigm when at zero temperature T the *I*-*V* curve is nonlinear (sub-Ohmic at small bias). In agreement with the LL theory, *ab initio* simulations of dislocations with superfluid cores reveal that LL parameters remain temperature independent at $T \lesssim 0.5$ K [15]. These observations resulted in a widely shared point of view that supertransport of ^{4}He atoms through the dislocation network is described by a bosonic LL [3,8]. However, at low finite T, the initial part of the otherwise temperature-independent *I*-*V* curve in LL is supposed to acquire an Ohmic regime characterized by high conductivity diverging in the $T \to 0$ limit as a power law. In contrast, experiments consistently observe a different mysterious temperature dependence of the critical flux F shown in Fig. 1 and, apparently, force one to look beyond isolated dislocations and invoke properties of the dislocation network (cf. Ref. [18]).

In this Letter, we argue that a single-dislocation scenario, where F is simply a product of the critical current J along one dislocation and a number of dislocations, is nevertheless possible by paying attention to the higher-dimensional nature of the problem—dislocations are defects of a three-dimensional crystalline order. In this context, two key ingredients become crucial: (i) thermal fluctuations of the dislocation shape and (ii) the exponential dependence of superfluid properties of the core on moderate changes in pressure (more generally, the stress field around the
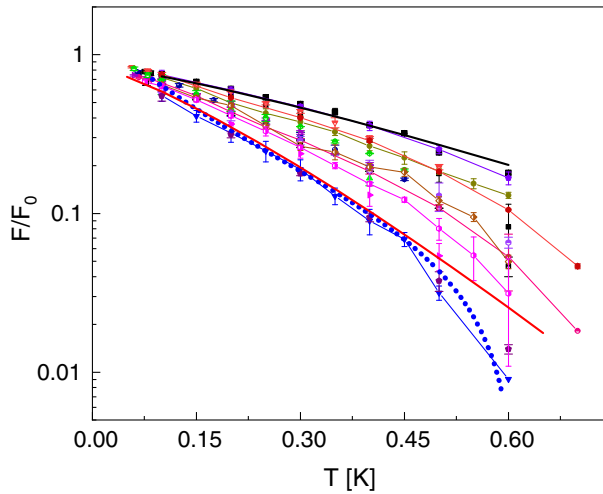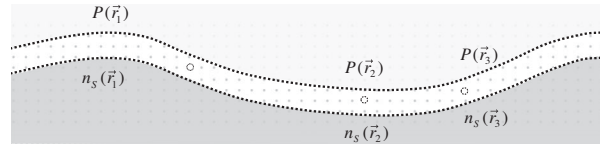
FIG. 2. Schematic visualization of shape fluctuations of the edge dislocation core in the climbing plane. The incomplete atomic plane is shown by the dark area with the core at its boundary. The superfluid density is confined to the core (between the dashed lines) and its local value strongly depends on the local pressure $P(\mathbf{r})$ (or stress).

FIG. 1. Critical flux $F(T)$ [normalized by $F_0 = F(T \approx 0)$] for differently grown ^{4}He samples. All data points connected by thin lines as a guide to the eye are taken from Refs. [5,6]. The dotted line represents the master curve, Ref. [1], fitting the data collected from multiple samples. In contrast to Refs. [5,6], the data from Ref. [1] show no spread within $\sim$10%. All the data for $T < 0.5$ K are consistent with the stretched exponential law $\exp[-(T/T_a)^\alpha]$, $\alpha = 1$–1.3, predicted by our model: The thick solid lines are fits with $\alpha = 5/4$ and $T_{5/4} \approx 0.20,\ 0.45$ K for the lowest and the highest datasets, respectively [5,6].

dislocation core)—as observed in the experiment [5] and in our simulations (see below). Their combination results in rare intermittent fluctuations with dislocation segments having strongly suppressed superfluid stiffness in what otherwise is a robust superfluid along the core. Phase slips in such regions limit the flux F. No other one-dimensional system is known to exhibit a similar behavior.

Our scenario is supported by *ab initio* and model simulations and explains the leading behavior observed in experiments; see Fig. 1. In particular, we explain finite size limitations of *ab initio* simulations and reveal strong suppression of the superfluid stiffness with pressure and temperature. Of direct relevance to experiments is, however, the critical current, which is out of reach for *ab initio* methods. We corroborate the scenario by a simplified effective model, which captures, at least qualitatively, the STS experiments that puzzled the community for over a decade. Given the spread of data for samples with different geometry, size, and growth conditions, it is natural to expect that our modeling will need further refinements: a group of samples from Ref. [6] follow a stretched exponential law with parameters outside of the range supported by our current model. In particular, our model does not capture the low-T saturation behavior seen in these samples. It also does not account for the sub-Ohmic dependence of the flux F on the chemical potential bias $\Delta\mu$ [2,6], which we leave for future work. The scope of the present Letter is hence limited to the unifying picture of the pressure and temperature dependence over a wide temperature range.

Scenario.—In solid ^{4}He the motion of atoms or vacancies along the dislocation core is best described by tunneling in the periodic potential (see the sketch, Fig. 2) implying exponential sensitivity of the superfluid properties to the potential strength. Quantum roughness of the superfluid edge dislocation renders thermal fluctuations of their shape gapless and, thus, anomalously large compared to the situation when the Peierls potential localizes the core within a single potential minimum. Shape fluctuations of the edge produce inhomogeneous stress fields along the core, which, in turn, modify the local superfluid response. Exponential sensitivity of tunneling phenomena to external parameters, such as the local stress, amplifies the effect.

Imagine an instant shape of the dislocation line being quenched. Transport properties of the resulting system are best described by the strong-disorder scenario [19–21] when special attention is paid to the statistics of rare regions (outliers in the pressure-stress distribution) creating "bottlenecks" that might determine the current. The dynamical nature of thermal fluctuations does not allow us to take this analogy literally; e.g., phase transitions at finite T are forbidden. Nevertheless, a sharp suppression of the superfluid density n_s and flux with temperature, see Fig. 1, is possible.

The difference between the two properties is that $n_s(T)$ dependence is a purely thermodynamic effect based on a macroscopic number of connected regions with suppressed local superfluid response, or weak regions (WR), while the critical current J_c (with $F \propto J_c$) is not. Because of the one-dimensional character of the system, J_c is determined by a *single* WR along the line allowing phase slips. The microscopic description of phase slips at WR goes beyond the scope of this work. However, for qualitative comparison with the experiment all we need are the following two natural assumptions. (i) J_c is a product of the local superfluid density $n_s(x)$ and the local critical velocity at WR. (ii) Phase slip is a ground-state, quantum-tunneling phenomenon often called an instanton. Smaller values of n_s lead to a smaller instanton action and, correspondingly, smaller critical velocities. Thus, we expect that J_c scales as a certain power ($p > 1$) of the local superfluid density n_s at the WR.

Here we do not consider thermal phase slips destroying the core superfluid in the thermally activated fashion [22] at
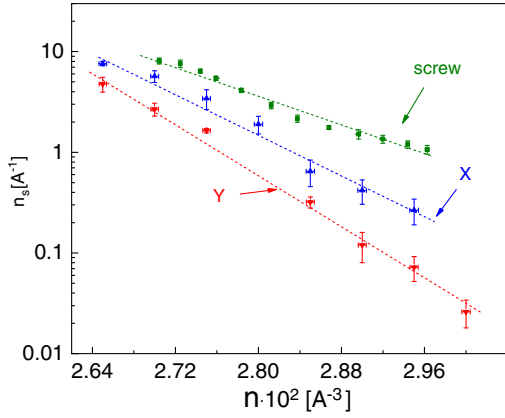
FIG. 3. Exponential sensitivity of the superfluid density in the dislocation core n_s to small changes in the 3D number density of the ^{4}He crystal n. Three different dislocations were simulated at $T = 0.25$ K: a screw dislocation and two edge dislocation partials along the [1,0,0] and [0,1,0] directions labeled as X and Y, respectively. Each data point corresponds to a different sample at the corresponding density. For more details see Ref. [15].

FIG. 4. Superfluid density $n_s(N)$ as a function of the deviation δN of the particle number N from its equilibrium expectation value $\langle N \rangle$ in the simulation cell for the superclimbing edge dislocation, at $T = 0.5$ K, and the screw dislocation with a superfluid core, at $T = 1$ K. The data are normalized by $\langle n_s \rangle$, which is n_s averaged over N.

higher temperatures. The corresponding activation energy E_0 is determined by $n_s(0)$ and the healing length ξ, and it can be estimated as $E_0 \approx \hbar^2 n_s(0)/(\xi m)$, where m is the ^{4}He atomic mass. Our *ab initio* simulations give $E_0 \sim 5$–10 K, which is much higher than the typical energy scale ~ 0.5 K observed experimentally in Refs. [1,5,6].

Ab initio simulations.—The key assumption is the exponential sensitivity of n_s to small changes in system parameters such as the crystal number density n. This was verified by *ab initio* Worm algorithm simulations [23] similar to those reported in Ref. [11] but at higher densities (see the Supplemental Material [15]): Figure 3 clearly shows that n_s can be suppressed by nearly 2 orders of magnitude with only a 10% change in n.

The largest simulated system linear size L cannot accommodate full-scale shape fluctuations of the dislocation because L does not satisfy the requirement $L \gg D_0$, where $D_0 \sim 10$ Å is the core diameter. However, rather than dealing with the shape fluctuations of a long dislocation line in an infinite ideal crystal, we can study the statistics of position fluctuations of a short dislocation—of length $L \sim 20$ Å $\gtrsim D_0$—within the box. Approximately, the dislocation can be viewed as composed of straight segments of length L, moving with respect to each other and interacting by elastic forces. The simulation box boundaries are formed by atoms with "frozen" spatial positions arranged to enforce the topology of the dislocation inside the box (see Ref. [15]). As a result, the interior is under stress gradients with the characteristic scale L. At the qualitative level, this arrangement mimics the effect of thermal shape fluctuations and allows us to study how the dislocation segment explores the nonuniform stress landscape and changes its superfluid properties depending on the position within the small box.
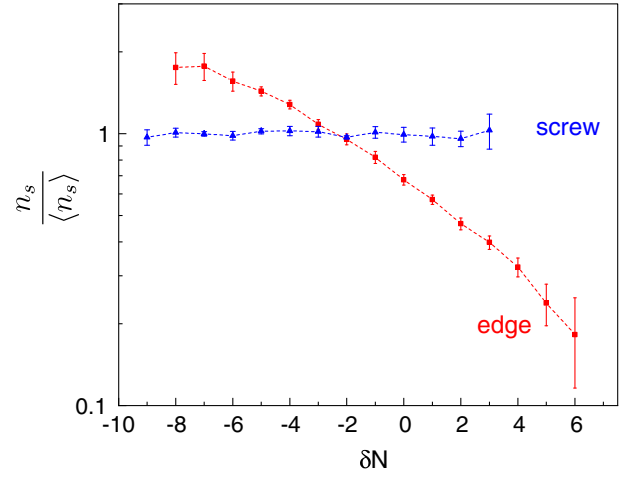
In the simulations, n_s is calculated through the variance of the winding number W [24]: $n_s = \hbar^{-2} m L T \langle W^2 \rangle$, where m is the particle mass, and $\langle \cdots \rangle$ stands for averaging over an ensemble of path-integral configurations. Large rare thermal fluctuations of the dislocation position are statistically insignificant in $\langle W^2 \rangle$ and this is why n_s stays T independent in short samples [15]. To reveal the effect of rare fluctuations one has to look at correlations between the W^2 and dislocation core position within the simulation cell, which can be readily done on the basis of the one-to-one correspondence between the edge dislocation position and the particle number N. This correspondence is the essence of the superclimb effect [11]: the position of the core with respect to the crystal boundary determines the number of extra atoms belonging to the incomplete atomic plane (the dark area in Fig. 2). Accordingly, fluctuations of the edge dislocation imply fluctuations of N. Note that there is no such relation for the screw dislocation. Since N is a constant of motion, its fluctuations are thermal, ensuring that we are studying finite T rather than zero-point effects.

In the numerical protocol, the parameters are chosen so that N experiences substantial fluctuations. The statistics of $\langle W^2 \rangle$ is then collected separately for each particle number N. The corresponding quantity is denoted as $\langle W^2 \rangle_N$ and defines the N-dependent superfluid density $n_s(N) = \hbar^{-2} m L T \langle W^2 \rangle_N$. If our scenario is correct, dramatic changes in $n_s(N)$ between typical and rare values of N should occur. The results are presented in Fig. 4. For large deviations of N from its expectation value $\langle N \rangle$ (that is, for large deviations of the core from its equilibrium position within the simulation cell), we observe significant (by a factor of ~ 5) changes in $n_s(N)$ (as compared with n_s averaged over N) for a superclimbing edge dislocation. In contrast, the screw dislocation with the

superfluid core experiencing similar fluctuations in N (which, however, cause no core displacement) demonstrates no dependence of $n_s(N)$ on N. This dramatic difference nicely illustrates the key aspect of our scenario for edge dislocations—the dependence on N is not due to particle density fluctuations within the superfluid core (as is the case for the screw dislocation), but due to the modification of the local crystalline environment around the climbing edge dislocation in the presence of the stress field gradients. The same conclusion follows from the direct comparison between Figs. 4 and 3 where both screw and edge dislocations demonstrate the exponential suppression with the crystal density n.

Model simulations.—Qualitatively, the shape fluctuations of the superclimbing edge dislocation and their effect on the superflow along its core can be studied within the simplified effective model of an isotropic string in two dimensions. That is, we ignore the presence of the crystalline lattice, which induces anisotropy and the Peierls potential. The effective Hamiltonian reads (in the units when the interatomic distance b and the ratio $\hbar/m$ equal to unity)

$$H[\varphi, y] = \frac{1}{2} \int_0^L dx \{n_s(y'')[V_0 + \varphi']^2 + Gy'^2\}, \quad (1)$$

where the superfluid phase field $\varphi(x)$ and the dislocation displacement field $y(x)$ are canonically conjugated variables. The term $\propto G$ is the elastic deformation energy. We consider the limit of small deviations of the line from its equilibrium $y(x) = 0$, that is, $|y'(x)| < 1$. Also, the line curvature $y''(x)$ must be much smaller than $1/D_0$. The kinetic energy part contains the average flux velocity V_0, and the local superfluid density,

$$n_s(y'') = n_0 \exp(-gy''), \quad (2)$$

which depends exponentially on the shape fluctuations through the line curvature y'' (see Refs. [13,15] for additional details). It is consistent with the dependence on pressure or density observed in the *ab initio* simulations presented in Figs. 3 and 4.

Quantum mechanical simulations of Eq. (1) at finite V_0 suffer from the sign problem. However, for purposes of qualitative analysis it is sufficient to consider the classical version of Eq. (1) with explicit temperature-dependent ultraviolet cutoff Δx on the wavelengths of excited modes for which quantization effects can be neglected. We implement the cutoff by working with the discretized version of Eq. (1) of linear size $\tilde{L} = L/\Delta x \gg 1$ and the noncompact field φ. Given that the spectrum of excitations is parabolic at small momenta [11], $\omega = \sqrt{n_0 G} q^2$ [11], we have $\Delta x \approx (n_0 G)^{1/4}/T^{1/2}$. This treatment is valid as long as $\Delta x \gg D_0$.
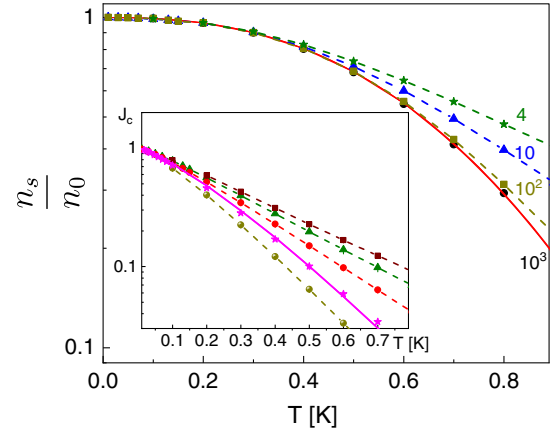

FIG. 5. Superfluid density n_s (dashed lines are guides to the eye) for linear sizes $\tilde{L}$ specified next to each dataset. The solid line is the fit by $\exp[-(T/T_\alpha)^\alpha]$, with $\alpha = 5/2$ and $T_\alpha = 0.737 \pm 0.005$. Inset: the critical current J_c (normalized to unity at $T = 0$) for $\tilde{L} = 4, 10, 10^2, 10^3, 10^4, 10^7$ increasing from the highest to the lowest dataset. The solid line is the fit of the $\tilde{L} = 10^4$ data by $J_c \propto \exp[-(T/T_\alpha)^{5/4}]$, with $T_\alpha = 0.257 \pm 0.01$. All data for J_c are consistent with $\alpha \approx 5/4 \pm 0.1$ for $0 < T < 0.6$ and the spread is due to T_α varying by a factor ~ 2 (cf. Fig. 1).

Brute-force classical simulations of Eq. (1) suffer from severe slowing-down because optimal WR configurations introduce strong and highly nonlocal correlations between the fields y and φ: A bump in the former is accompanied by a large gradient in the latter at the bump location with reduced φ gradients everywhere else. Stochastic sampling of optimal WR configurations thus requires an enormous number of elementary local moves. However, for purposes of the semiquantitative analysis, the slowing-down problem can be solved by implementing the least-energy approximation for the field $\varphi(x)$ when $\varphi(x)$ is nothing but the optimal solution for a given configuration of $y(x)$. In practice, this approximation reduces to an effective energy functional that depends only on $y(x)$, which is then sampled stochastically. The optimal phase field solution corresponds to the constant current condition:

$$J = n_s(y''(x))[V_0 + \varphi'(x)], \qquad dJ/dx = 0. \quad (3)$$

The superfluid density n_s is computed from $n_s = \langle J \rangle / V_0$ in the $V_0 \to 0$ limit. The critical flux $F \propto J_c$ cannot be determined from equilibrium Monte Carlo simulations. Nevertheless, the origin of its T dependence can be traced back to the statistics of the WR through the proposed dependence of J_c on superfluid density in WR:

$$J_c \propto \langle n_s^p \rangle_W \propto \langle \exp(-pgy'') \rangle_W. \quad (4)$$

Here $\langle \cdots \rangle_W$ denotes averaging over the WR. (Note that an alternative interpretation in terms of the Landau criterion

for stability of the superflow is also possible [15].) The results of the simulations for n_s and J_c with $p = 2$ are presented in Fig. 5 (see also Fig. 1), with further technical details delegated to the Supplemental Material [15].

Conclusions and outlook.—Superflow-through-solid experiments exhibit a highly unusual temperature dependence of the critical flux (see Fig. 1) that does not conform with the standard Luttinger liquid theory expected to work within the otherwise consistent and numerically corroborated picture of superfluidity confined to dislocation cores. Our scenario provides an explanation: the one-dimensional superfluid channel is an inseparable part of the crystalline host and its shape fluctuations induce pressure-stress and density fluctuations modifying properties of the edge dislocation core (see Fig. 4). Since superfluidity comes from tunneling motion of core atoms in the periodic crystal potential, the net result is an exponential dependence of n_s on small changes in P, and, consequently, in combination with the thermal fluctuations—on T.

The long-wave physics of rough superfluid edge dislocations is captured by the effective model (1). It reveals the effect of rare shape fluctuations on the superfluid density and emphasizes a nearly classical nature of these fluctuations up to two quantum effects: (i) the UV cutoff on the wavelength of shape fluctuations and (ii) the value of the largest ground-state flux limited by phase slips (this quantum-tunneling phenomenon still remains to be understood).

The sharp temperature dependence of the critical flux is attributed to a single weakest region along the dislocation. Phenomenological treatment based on the assumption that the critical flux scales as a certain power (larger than one) of the local superfluid density at the weakest element allows us to reproduce experimental results at $T \leq 0.5$ K; see Fig. 1. At higher temperature the data in Fig. 1 decay faster; this can be accounted for by considering the contribution of bulk phonons to shape fluctuations, which leads to $\ln(F/F_0) \sim -T^2$ [15].

The quantum treatment of Eq. (1) is of fundamental interest on its own because it describes a new type of the quasi-1D superfluid—not accounted for by the Luttinger liquid paradigm.

The inset in Fig. 5 demonstrates weak (logarithmic) suppression of the critical flux with increasing the dislocation length. A similar suppression of the flux with the sample size has been reported in Ref. [6]. This motivates further experimental studies of the STS effect in single crystals with variable distance between the Vycor "electrodes". If crystals can be grown with predominantly screw dislocations, the genuine Luttinger liquid behavior can be revealed through the temperature-independent supercritical flux (at low temperature).

[1] M. W. Ray and R. B. Hallock, Phys. Rev. Lett. **100**, 235301 (2008); Phys. Rev. B **79**, 224302 (2009); M. W. Ray and R. B. Hallock, Phys. Rev. B **81**, 214523 (2010).

[2] Ye. Vekhov and R. B. Hallock, Phys. Rev. Lett. **109**, 045303 (2012).

[3] R. B. Hallock, J. Low Temp. Phys. **197**, 167 (2019).

[4] Z. G. Cheng, J. Beamish, A. D. Fefferman, F. Souris, S. Balibar, and V. Dauvois, Phys. Rev. Lett. **114**, 165301 (2015); Z. G. Cheng and J. Beamish, Phys. Rev. Lett. **117**, 025301 (2016).

[5] J. Shin, D. Y. Kim, A. Haziot, and M. H. W. Chan, Phys. Rev. Lett. **118**, 235301 (2017).

[6] J. Shin and M. H. W. Chan, Phys. Rev. B **99**, 140502(R) (2019).

[7] J. Shin and M. H. W. Chan, Phys. Rev. B **101**, 014507 (2020).

[8] M. H. W. Chan, J. Low Temp. Phys. **205**, 235 (2021).

[9] A. Haziot, X. Rojas, A. D. Fefferman, J. R. Beamish, and S. Balibar, Phys. Rev. Lett. **110**, 035301 (2013).

[10] M. Boninsegni, A. B. Kuklov, L. Pollet, N. V. Prokof'ev, B. V. Svistunov, and M. Troyer, Phys. Rev. Lett. **99**, 035301 (2007).

[11] S. G. Söyler, A. B. Kuklov, L. Pollet, N. V. Prokof'ev, and B. V. Svistunov, Phys. Rev. Lett. **103**, 175301 (2009).

[12] S. I. Shevchenko, Fiz. Nizk. Temp. **13**, 115 (1987) [Sov. J. Low Temp. Phys. **13**, 61 (1987)].

[13] P. M. Anderson, J. P. Hirth, and J. Lothe, *Theory of Dislocations* (Cambridge University Press, Cambridge, England, 2017).

[14] D. Hull and D. J. Bacon, *Introduction to Dislocations* (Elsevier, Amsterdam, 2011).

[15] See Supplemental Material at http://link.aps.org/supplemental/10.1103/PhysRevLett.128.255301 for details of the dislocation structure, sample preparation, and simulations, which includes Refs. [16,17].

[16] M. Yarmolinsky and A. B. Kuklov, Phys. Rev. B **96**, 024505 (2017); Longxiang Liu and A. B. Kuklov, Phys. Rev. B **97**, 104510 (2018).

[17] D. S. Greywall, Phys. Rev. B **16**, 5127 (1977).

[18] A. B. Kuklov, N. V. Prokof'ev, and B. V. Svistunov, Physics **4**, 109 (2011).

[19] E. Altman, Y. Kafri, A. Polkovnikov, and G. Refael, Phys. Rev. Lett. **93**, 150402 (2004); Phys. Rev. B **81**, 174528 (2010).

[20] L. Pollet, N. V. Prokof'ev, and B. V. Svistunov, Phys. Rev. B **89**, 054204 (2014).

[21] Z. Yao, L. Pollet, N. V. Prokof'ev, and B. V. Svistunov, New J. Phys. **18**, 045018 (2016).

[22] J. S. Langer and V. Ambegaokar, Phys. Rev. **164**, 498 (1967).

[23] M. Boninsegni, N. Prokof'ev, and B. Svistunov, Phys. Rev. Lett. **96**, 070601 (2006); Phys. Rev. E **74**, 036701 (2006).

[24] E. L. Pollock and D. M. Ceperley, Phys. Rev. B **36**, 8343 (1987).